



HAL
open science

Calcium signaling mediates a biphasic mechanoadaptive response of endothelial cells to cyclic mechanical stretch

Yekaterina Miroshnikova, Sandra Manet, Xinping Li, Sara Wickström, Eva Faurobert, Corinne Albiges-Rizo

► **To cite this version:**

Yekaterina Miroshnikova, Sandra Manet, Xinping Li, Sara Wickström, Eva Faurobert, et al.. Calcium signaling mediates a biphasic mechanoadaptive response of endothelial cells to cyclic mechanical stretch. *Molecular Biology of the Cell*, 2021, 32 (18), pp.1724-1736. <10.1091/mbc.E21-03-0106>. <hal-03409570>

HAL Id: hal-03409570

<https://hal.science/hal-03409570v1>

Submitted on 17 Nov 2021

HAL is a multi-disciplinary open access archive for the deposit and dissemination of scientific research documents, whether they are published or not. The documents may come from teaching and research institutions in France or abroad, or from public or private research centers.

L'archive ouverte pluridisciplinaire **HAL**, est destinée au dépôt et à la diffusion de documents scientifiques de niveau recherche, publiés ou non, émanant des établissements d'enseignement et de recherche français ou étrangers, des laboratoires publics ou privés.



HAL Authorization

Calcium signaling mediates a biphasic mechanoadaptive response of endothelial cells to cyclic mechanical stretch

Yekaterina A. Miroshnikova^{a,b,c,d,e,f,g,*}, Sandra Manet^{a,b,c,†}, Xiping Li^d, Sara A. Wickström^{d,e,f,g}, Eva Faurobert^{a,b,c,†}, and Corinne Albiges-Rizo^{a,b,c,†}

^aUniversité Grenoble Alpes, Institute for Advanced Biosciences, Grenoble 38042, France; ^bINSERM U1209 and ^cCNRS UMR 5039, Institute for Advanced Biosciences, F-38700 La Tronche, France; ^dMax Planck Institute for Biology of Ageing, D-50931 Cologne, Germany; ^eHelsinki Institute of Life Science and ^fWihuri Research Institute, Biomedicum Helsinki, and ^gStem Cells and Metabolism Research Program, Faculty of Medicine, University of Helsinki, FI-00014 Helsinki, Finland

ABSTRACT The vascular system is precisely regulated to adjust blood flow to organismal demand, thereby guaranteeing adequate perfusion under varying physiological conditions. Mechanical forces, such as cyclic circumferential stretch, are among the critical stimuli that dynamically adjust vessel distribution and diameter, but the precise mechanisms of adaptation to changing forces are unclear. We find that endothelial monolayers respond to cyclic stretch by transient remodeling of the vascular endothelial cadherin-based adherens junctions and the associated actomyosin cytoskeleton. Time-resolved proteomic profiling reveals that this remodeling is driven by calcium influx through the mechanosensitive Piezo1 channel, triggering Rho activation to increase actomyosin contraction. As the mechanical stimulus persists, calcium signaling is attenuated through transient down-regulation of Piezo1 protein. At the same time, filamins are phosphorylated to increase monolayer stiffness, allowing mechanoadaptation to restore junctional integrity despite continuing exposure to stretch. Collectively, this study identifies a biphasic response to cyclic stretch, consisting of an initial calcium-driven junctional mechanoreponse, followed by mechanoadaptation facilitated by monolayer stiffening.

Monitoring Editor

Alpha Yap
University of Queensland

Received: Mar 8, 2021

Revised: May 10, 2021

Accepted: May 27, 2021

This article was published online ahead of print in MBoC in Press (<http://www.molbiolcell.org/cgi/doi/10.1091/mbc.E21-03-0106>) on June 3, 2021.

[†]These authors contributed equally to this work.

[†]Deceased.

Author contributions: Y.A.M. conceived the project, designed and performed most of the experiments, and analyzed data. S.M. designed constructs and performed experiments. X.L. performed proteomics analyses. S.A.W. designed experiments and analyzed data. E.F. and C.A.R. supervised project, designed experiments, and analyzed data. Y.A.M. and S.A.W. wrote the paper. All authors commented on and edited the manuscript.

Competing interests: The authors declare no competing interests.

*Address correspondence to: Yekaterina A. Miroshnikova (yekaterina.miroshnikova@helsinki.fi).

Abbreviations used: AJ, adherens junction; BioID, proximity-dependent biotin identification; EC, endothelial cells; HUVEC, human umbilical vascular endothelial cells; LFO, label-free quantification; PAK, p21-activated kinase; pMLC2, phosphorylated myosin light chain-2; VE-cadherin, vascular endothelial cadherin.

© 2021 Miroshnikova et al. This article is distributed by The American Society for Cell Biology under license from the author(s). Two months after publication it is available to the public under an Attribution-Noncommercial-Share Alike 3.0 Unported Creative Commons License (<http://creativecommons.org/licenses/by-nc-sa/3.0>).

"ASCB®," "The American Society for Cell Biology®," and "Molecular Biology of the Cell®" are registered trademarks of The American Society for Cell Biology.

INTRODUCTION

The vasculature, lined by specialized epithelial cells termed endothelial cells (ECs), is one of the most dynamic and inherently mechanically loaded tissues, with mechanical inputs ranging from fluid shear stress to compression and stretch. These inputs arise from pulsatile fluid flow and contraction activity of surrounding smooth muscle cells, pushing and pulling forces resulting from transmigration of immune cells, and hydrostatic compression and mechanical properties of the basement membrane that underlies the EC monolayer (Hahn and Schwartz, 2009; Dorland and Huvener, 2017).

Fluid shear stress, the frictional force per unit area from flowing blood, and circumferential stretch, which arises mainly from blood pressure, are generally considered the most relevant forces acting on ECs (Hahn and Schwartz, 2009). Typical magnitudes of fluid shear stress in mammalian blood vessels range between 0.5 and 5 Pa (Lipowsky et al., 1978), whereas traction forces from ECs to the extracellular matrix in vitro are around 100 Pa (Krishnan et al., 2011). In contrast, stress from circumferential stretching of the vessel wall during the cardiac cycle can exceed 1000 Pa (Haga et al., 2007), thereby representing the strongest extrinsic force experienced by ECs.

The mechanical environment of the endothelium is constantly changing, depending on the physical activity status of the body and various hormonal inputs that affect blood pressure and vascular tone (Logsdon *et al.*, 2014; Baeyens and Schwartz, 2016). These dynamic forces are sensed by a number of mechanosensitive proteins expressed by the ECs. Many putative mechanotransducers have been proposed to function in sensing stretch, including ion channels, integrins, receptor tyrosine kinases, heterotrimeric G proteins, platelet-endothelial-cell adhesion molecule-1, and vascular endothelial (VE)-cadherin (Hahn and Schwartz, 2009; Dorland and Huveneers, 2017). Thus cell–matrix and cell–cell adhesions play critical roles in mechanotransduction. Both of these adhesive sites are directly coupled to the actin, microtubule, and intermediate filament cytoskeletons. This direct coupling allows transmission of extrinsic forces into the cell to trigger mechanosensitive signals that subsequently alter cytoskeletal structures either directly or via gene expression changes (Hoffman *et al.*, 2011; Iskratsch *et al.*, 2014).

Although the molecular components that allow ECs to respond to cyclic stretch are relatively well known, it is not clear how the adhesive and contractile machineries respond to rapid changes in extrinsic mechanical forces to resist external forces and thereby prevent cell shape deformation. In addition, the mechanisms of sustained adaptive responses to the new mechanical environment are unclear. Here we report that cyclic mechanical stretch triggers calcium signaling through the stretch-induced ion channel Piezo1 to activate cytoskeletal contractility that leads to transient VE-cadherin junction remodeling. Sustained stretch, however, leads to degradation of Piezo and attenuation of calcium influx. At the same time, filamin actin cross-linkers remodel the actin cytoskeleton to increase EC cortical stiffness. This facilitates restoration of junction integrity in the presence of continuous high stretch.

RESULTS

Cyclic mechanical stretch triggers transient adherens junction remodeling and actomyosin contraction

To investigate how EC monolayers adapt to dynamic changes in their mechanical microenvironment, we exposed human umbilical vascular endothelial cells (HUVEC) to cyclic biaxial mechanical stretch within the physiological range (20%, 100–1200mHz; Jufri *et al.*, 2015; Figure 1A). Time-resolved analyses of HUVEC monolayers using immunofluorescence revealed that within 30 min of stretch, marked morphological changes occurred at adherens junctions (AJs), characterized by widening of intercellular spacing and transformation of linear cell–cell contacts into zipper-like irregular contacts, a morphology characteristic of junctions under high tension (Dorland and Huveneers, 2017; Figure 1, B–D). Consistent with this notion of increased tension, we observed up-regulation of phosphorylated myosin light chain-2 (pMLC2; Figure 1, B and D) indicative of increased actomyosin contractility. In addition, the tension-sensitive epitope of the actin-binding adaptor at VE-cadherin junctions, α 18-catenin (Yonemura *et al.*, 2010), showed increased accessibility at 30 min of stretch (Figure 1, E and F). Vinculin staining as an additional readout for AJ mechanosignaling (Twiss *et al.*, 2012; Konishi *et al.*, 2019) showed increased presence of vinculin at both cell–cell and cell–matrix adhesions at 30 min of stretch (Supplemental Figure 1, A and B), consistent with observations of vinculin recruitment to AJs under tension (le Duc *et al.*, 2010; Huveneers *et al.*, 2012). Importantly, no major changes in cell size or shape were observed (Supplemental Figure 1, C and D). Interestingly, the remodeling of adhesions and actomyosin contractility peaked at 30–60 min of stretch, but these changes were fully restored to baseline at 3 h of stretch (Figure 1, B–F), indicative of monolayer adaptation to the

continuous cyclic stretch. Similar effects were observed also with higher stretch frequencies (600 and 1200 mHz; Supplemental Figure 1, E and F). Collectively these data indicated that stretch triggered transient and reversible mechanical remodeling and increased tension at VE-cadherin junctions, whereas cell shapes were maintained, indicative of ability of the monolayers to resist extrinsic forces.

Adherens junction remodeling and reinforcement is associated with subtle changes in the vascular endothelial cadherin interactome

To understand how VE-cadherin junction morphology could be reestablished despite the presence of continuous mechanical stretch, we hypothesized that the composition of these junctions could be altered to recruit proteins with abilities to mechanically stabilize junctions. To quantify junction composition in the steady state and in the presence of stretch, we expressed VE-cadherin fused to biotin ligase (VE-Cad-BioID2) in HUVECs and utilized mass spectrometry to identify and quantify proximally localized proteins that were biotinylated (Figure 2, A and B). The most abundant of the 135 proteins identified as significantly enriched compared with biotin ligase controls in non-stretched HUVEC monolayers were catenins and other known components of cell–cell contacts such as vinculin and cingulin (Figure 2, C and D). Other significantly enriched proteins included regulators of AJs, cytoskeleton, trafficking, or signaling (Supplemental Table 1). In addition to structural components, several signaling proteins, in particular components of the Rho and Rac GTPase pathways, were detected. These included p21-activated kinase-4 (PAK4) and multiple GTPase activating proteins and guanine nucleotide exchange factors (Figure 2C; Supplemental Table 1). Interestingly, the molecular composition of the VE-cadherin did not differ substantially between control and stretch conditions, with only 20 proteins differentially abundant at 30 min and 32 proteins altered at 3 h (FDR < 0.05; Supplemental Figure 2, B and C; Supplemental Table 1). Most differentially abundant proteins were related to mechanical reinforcement of junctions, such as vinculin, integrin-linked kinase (Vespa *et al.*, 2005; le Duc *et al.*, 2010; Dufour *et al.*, 2013; Kim and Cooper, 2018). These analyses strengthened the conclusion that junctions are mechanically reinforced at 30–60 min of stretch. However, the limited number of changes indicated that alterations in the molecular composition of VE-cadherin junctions likely do not fully explain mechanical remodeling and restoration of junctions upon stretch.

Phosphoproteome analyses implicate activation of RhoA and Rac-PAK1 signaling and subsequent cytoskeletal remodeling upon stretch

We next asked what type of upstream signaling events would trigger the observed junctional/cytoskeletal remodeling and mechanoadaptation. To this end, we performed quantitative phosphoproteome analyses of cells exposed to 0, 30, and 60 min of 20% stretch (Figure 3A). During this time, no major alterations in the total proteome of cells was observed (only 20 proteins altered with padjust < 0.05; Supplemental Table 2). Intriguingly, we observed substantial changes in the phosphoproteome upon stretch (Figure 3B; Supplemental Tables 3 and 4). In particular, multiple components of the RhoA and PAK-Rac-Git signaling axes (Zhang *et al.*, 2011; van Buul *et al.*, 2014), which were also enriched in the VE-cadherin adhesion, were differentially phosphorylated after 30 min of stretch (Figure 3, C and D; Supplemental Table 3). In addition, a large number of cytoskeletal regulators were found to be differentially phosphorylated (Figure 3, C and D). Interestingly, upon 60 min of stretch, two actin cross-linkers, filamin A and B, became increasingly phosphorylated (Figure 3, C and E; Supplemental Table 4).

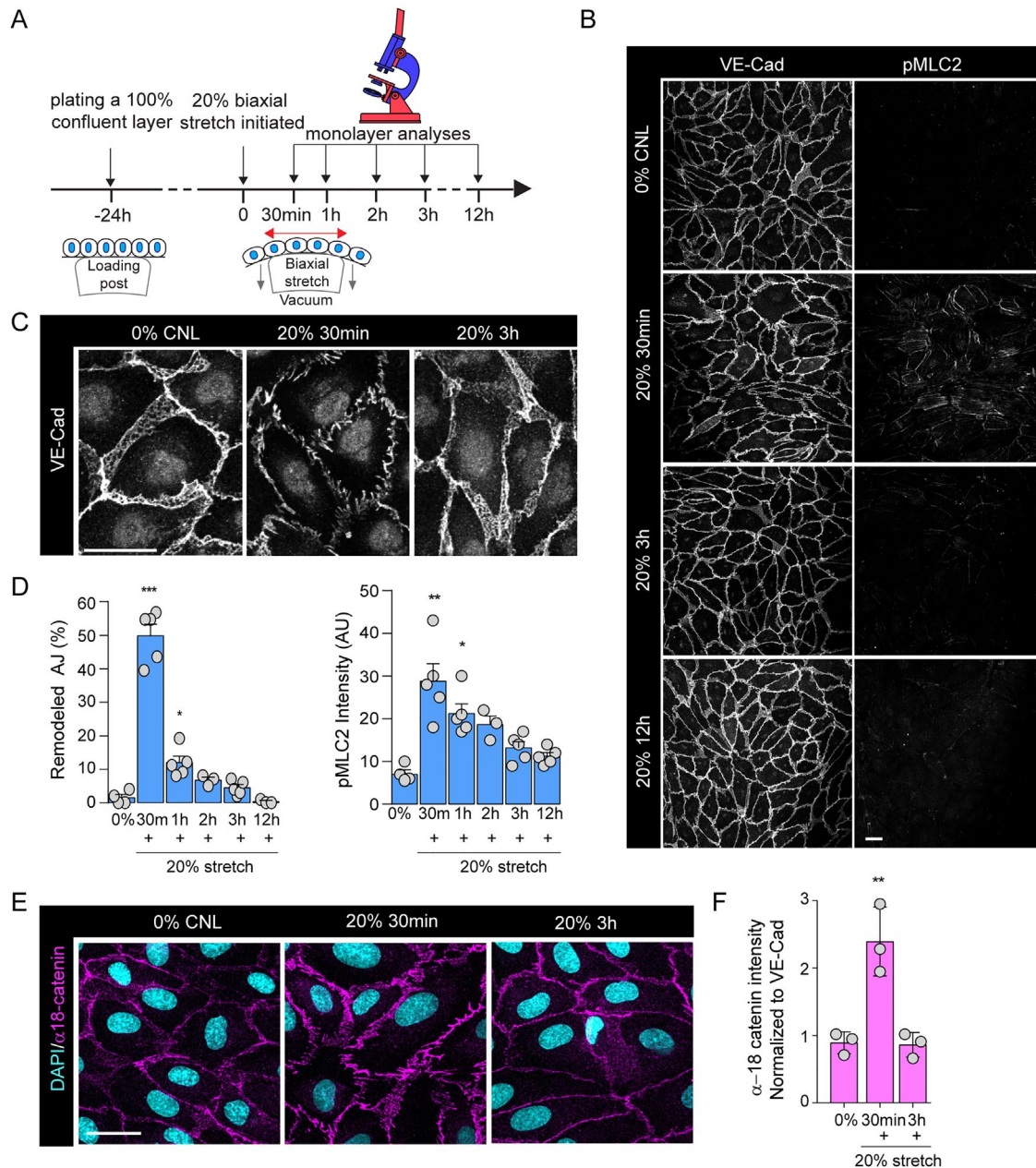


FIGURE 1: Cyclic mechanical stretch triggers transient adherens junction remodeling and actomyosin contraction. (A) Schematic illustration of stretch experiments. HUVECs were plated at confluency on silicon elastomers 24 h before stretch application, using negative pressure to deform the elastomer substrates (20%, 100 mHz), after which monolayers were analyzed at time points indicated. (B) Representative immunofluorescence images of VE-cadherin (VE-Cad) and pMLC2-stained HUVEC monolayers exposed to stretch. Note transient emergence of zipper-patterned adhesions and increased pMLC signal at 30 min of stretch. Scale bars 30 μ m. (C) Close-up images of junctional rearrangements show reversibility of junctional zipping upon stretch. Scale bars 30 μ m. (D) Quantification of AJ remodeling from VE-cadherin staining (left panel) and pMLC2 intensity (right panel). Mean \pm SEM; $n = 5$ independent experiments; *** $p = 0.0006$, * $p = 0.0203$ (VE-cadherin) and * $p = 0.0168$ and * $p = 0.0071$ (pMLC2), ANOVA, Dunnett's. (E) Representative immunofluorescence images of α -18-stained HUVEC monolayers exposed to stretch. Note transient increase in α -18 intensity at 30 min of stretch. Scale bars 30 μ m. (F) Quantification of α -18 catenin normalized to VE-cadherin intensity. Mean \pm SD; $n = 3$ independent experiments; ** $p = 0.0018$, ANOVA, Dunnett's.

Collectively this indicated that cyclic stretch triggered substantial changes in phosphorylation of components of cell–cell contacts and the cytoskeleton, with prominent changes in the RhoA and Rac-PAK pathways occurring at 30 min stretch, temporally coinciding with junction remodeling, and filamin phosphorylation at 60 min of stretch, temporally coinciding with junction restoration.

Stretch triggers transient calcium signaling and activation of Rho and Rac GTPases to remodel junctions

As the phosphoproteome implied involvement of GTPase signaling in the early phases of the stretch response, we next investigated the activities of these pathways in more detail. We performed time-resolved GTPase activity assays for RhoA and Rac GTPases and found

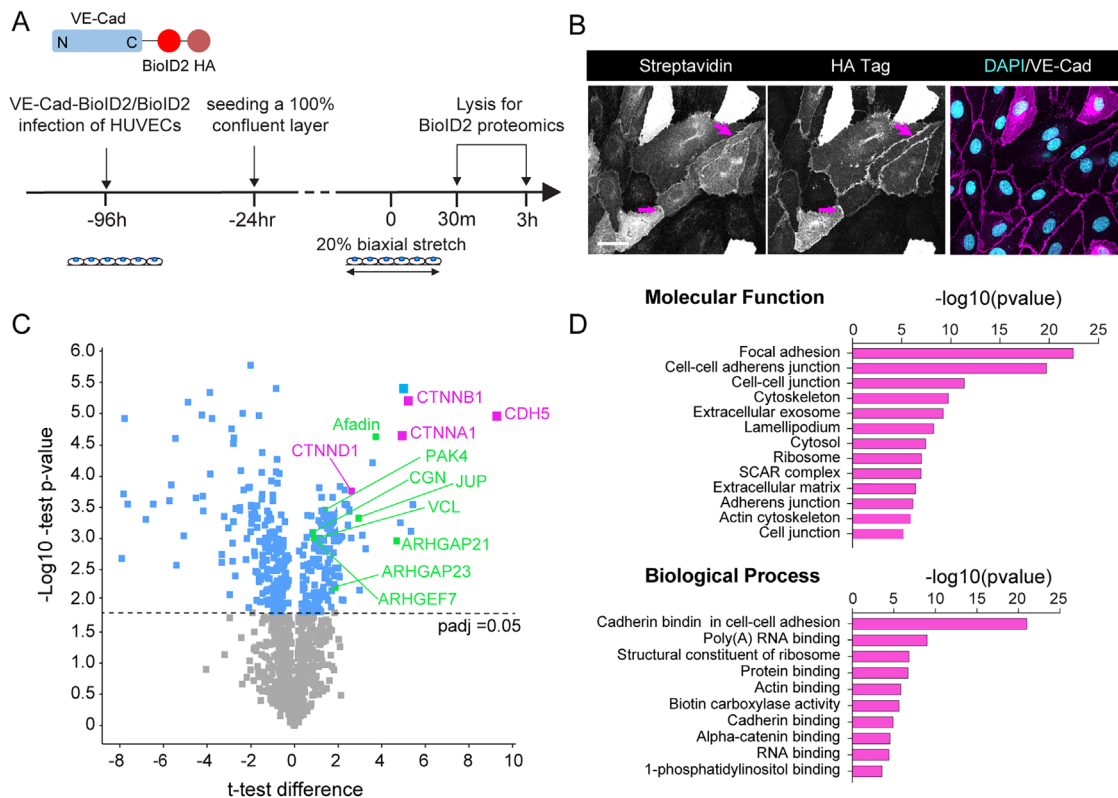


FIGURE 2: AJ remodeling and reinforcement is associated with subtle changes in VE-cadherin interactome. (A) Schematic illustration of VE-cadherin (VE-Cad)-BioID2 pull-down and mass spectrometry to identify stretch-dependent interactome changes. (B) Representative immunofluorescence images showing localization of HA-tagged VE-cadherin-BioID2 at AJs and enrichment of streptavidin as a result of biotin binding at this site. Scale bars 30 μ m. (C) Volcano plot of protein enrichment in VE-cadherin-BioID2 compared with BioID2 control. Note enrichment of VE-cadherin itself (*CDH5*) along with α - and β -catenin (*CTNNA1*, *CTNNB1*), indicative of successful enrichment of AJ components. Also highlighted are cytoskeletal and adhesion remodelers. Dotted line marks padj cutoff of 0.05, moderated t test/Benjamini Hochberg. (D) GO term enrichment analysis of proteins significantly enriched in VE-cadherin-BioID2 pull-downs.

that RhoA was rapidly and transiently activated after 10 min of stretch (Figure 4A; Supplemental Figure 3A), temporally coinciding with initiation with increase in contractility (Figure 1). In contrast, Rac showed slightly slower activation kinetics and the activity persisted up to 30 min (Figure 4B; Supplemental Figure 3B), also when the restoration of junctions was initiated (Figure 1). We hypothesized that RhoA could be upstream of increased actomyosin contractility and junctional tension, whereas Rac1 could function to restore junction stability as reported previously (Daneshjou *et al.*, 2015; Acharya *et al.*, 2018). Thus, to test if the activation of Rho and Rac pathways was responsible for junction remodeling and restoration, respectively, we inhibited the key downstream effectors of these pathways using a ROCK inhibitor, Y-27632, and a PAK1 inhibitor, IPA3. As expected (Brzeska *et al.*, 2004; Ohgushi *et al.*, 2010), inhibition of Rac induced pMLC2 and thus junctional remodeling already in steady state non-stretched monolayers, whereas Y-27632 prevented attenuated pMLC2 (Supplemental Figure 3E). Immunofluorescence analyses further revealed that stretch-induced VE-cadherin remodeling was indeed dependent on ROCK activity, whereas inhibition of PAK1 attenuated junction restoration (Figure 4C). We hypothesized that RhoA-mediated increased cell contractility and increased junctional tension could function to allow cells to resist deformation in response to stretch. To test this, we quantified cell area in stretched cells and noted a marked increase in cell spread area in Y-27632 treated monolayers, but not in control monolayers (Supplemental Figure 3C).

We next sought to investigate the upstream mechanosensor that could control junctional remodeling. As both Rac and Rho have been shown to be activated by calcium (Price *et al.*, 2003; Sakurada *et al.*, 2003), we proceeded to investigate changes in intracellular calcium in response to stretch. Analysis of an intracellular calcium reporter dye (Fluo-4-AM; Lock *et al.*, 2015) showed increased intracellular calcium levels emerging after 5 min of stretch and peaking at 30 min. Surprisingly, despite the continuous presence of stretch, intracellular calcium levels were back to baseline after 3 h of stretch (Figure 4, D and E). As elevation of intracellular calcium coincided temporally with junction remodeling, we next asked if calcium influx would be sufficient to trigger junction remodeling. To this end, we treated cells with the calcium ionophore ionomycin (Liu and Hermann, 1978; Supplemental Figure 3D) and analyzed the dynamics of VE-cadherin using live imaging of VE-cadherin-Apple. Analysis of the imaging data revealed junctional remodeling within seconds to minutes of addition of ionomycin (Figure 4F). Taken together, these experiments showed that stretch activates RhoA to drive myosin dependent contractility and junction remodeling, followed by Rac-mediated junctional restoration. Further, stretch triggers a rapid calcium influx that is capable of triggering junction remodeling.

Stretch reduces Piezo1 levels to attenuate calcium signaling

We hypothesized that mechanosensitive ion channels could be responsible for elevation of intracellular calcium upon stretch. Indeed,

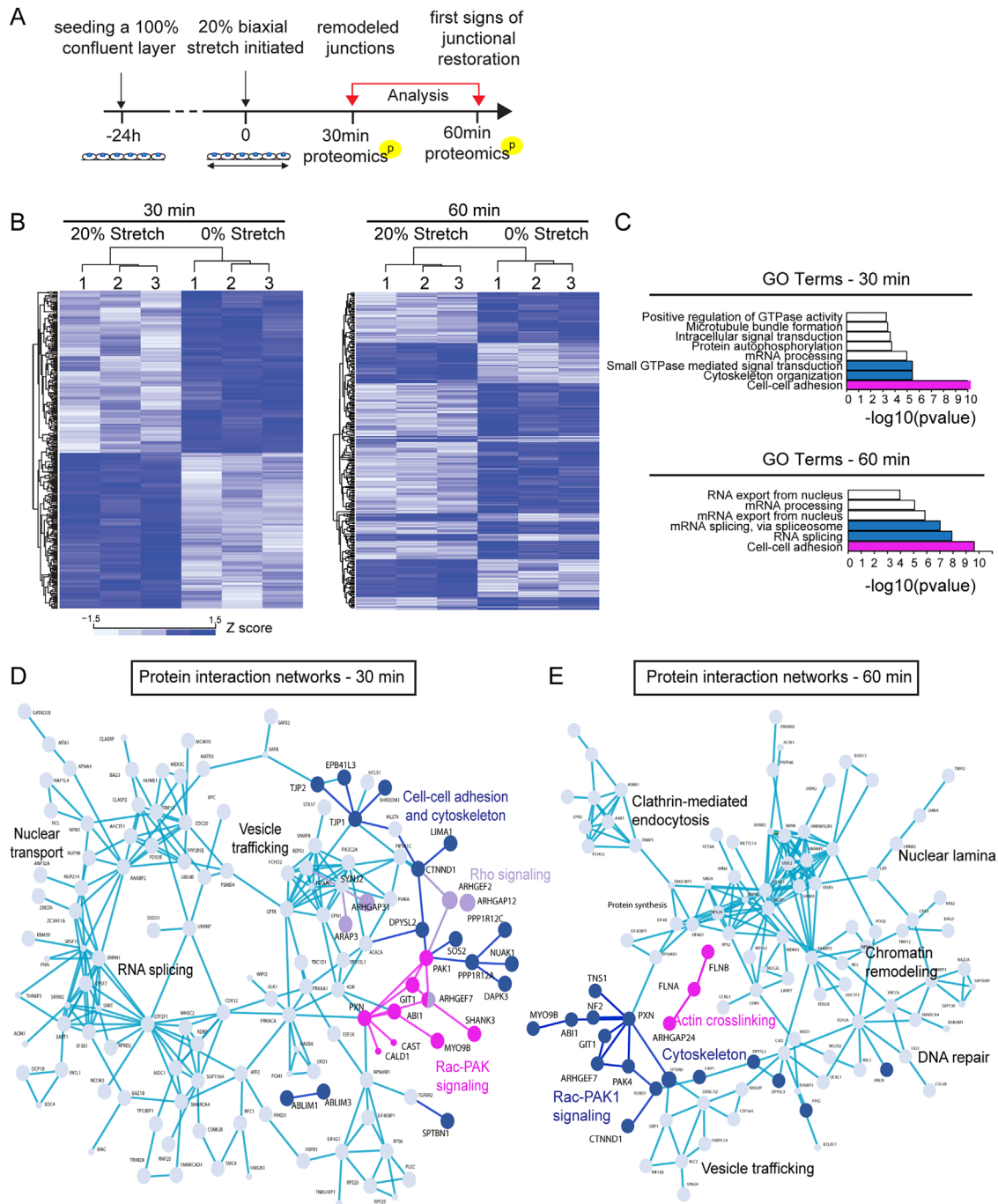


FIGURE 3: Phosphoproteome analyses implicate activation of RhoA and Rac-PAK1 signaling and subsequent cytoskeletal remodeling upon stretch. (A) Schematic illustration of the timeline of the phosphoproteome analyses. (B) Heat map and Euclidean distance-based clustering of differentially phosphorylated proteins at 30 min (left panel) and 60 min (right panel) of stretch. At 30 min, 185 up-regulated and 193 down-regulated phosphorylations are detected, and at 60 min, 86 up-regulated and 190 down-regulated phosphorylations are detected. (C) Protein–protein interaction network analysis (STRING) of differentially phosphorylated proteins at 30 min. Various components of the Rho A (purple) and Rac-Pak (magenta) signaling pathways as well as cytoskeletal and cell–cell adhesion regulators (dark blue) are identified. (D) GO term enrichment analyses of differentially phosphorylated proteins show enrichment of components and regulators of cell–cell adhesions both at 30 and 60 min. In addition, cytoskeletal organization and small GTPases are enriched at 30 min, whereas mRNA splicing is enriched at 60 min. (E) Protein–protein interaction network analysis of differentially phosphorylated proteins at 60 min. Various components of the Rac-Pak signaling pathway, cytoskeletal and cell–cell adhesion regulators (all in dark blue), and filamins (magenta) are identified.

inhibiting stretch-induced ion channels by GsMTx4 (Bae et al., 2011) prevented junction remodeling in response to stretch (Figure 5, A and B). To investigate the potential role of Piezo1, a key mechano-

sensitive calcium channel in the cardiovascular system (Beech and Kalli, 2019) that was also regulated in our phosphoproteome analysis, we depleted it using siRNA (Supplemental Figure 4A) and

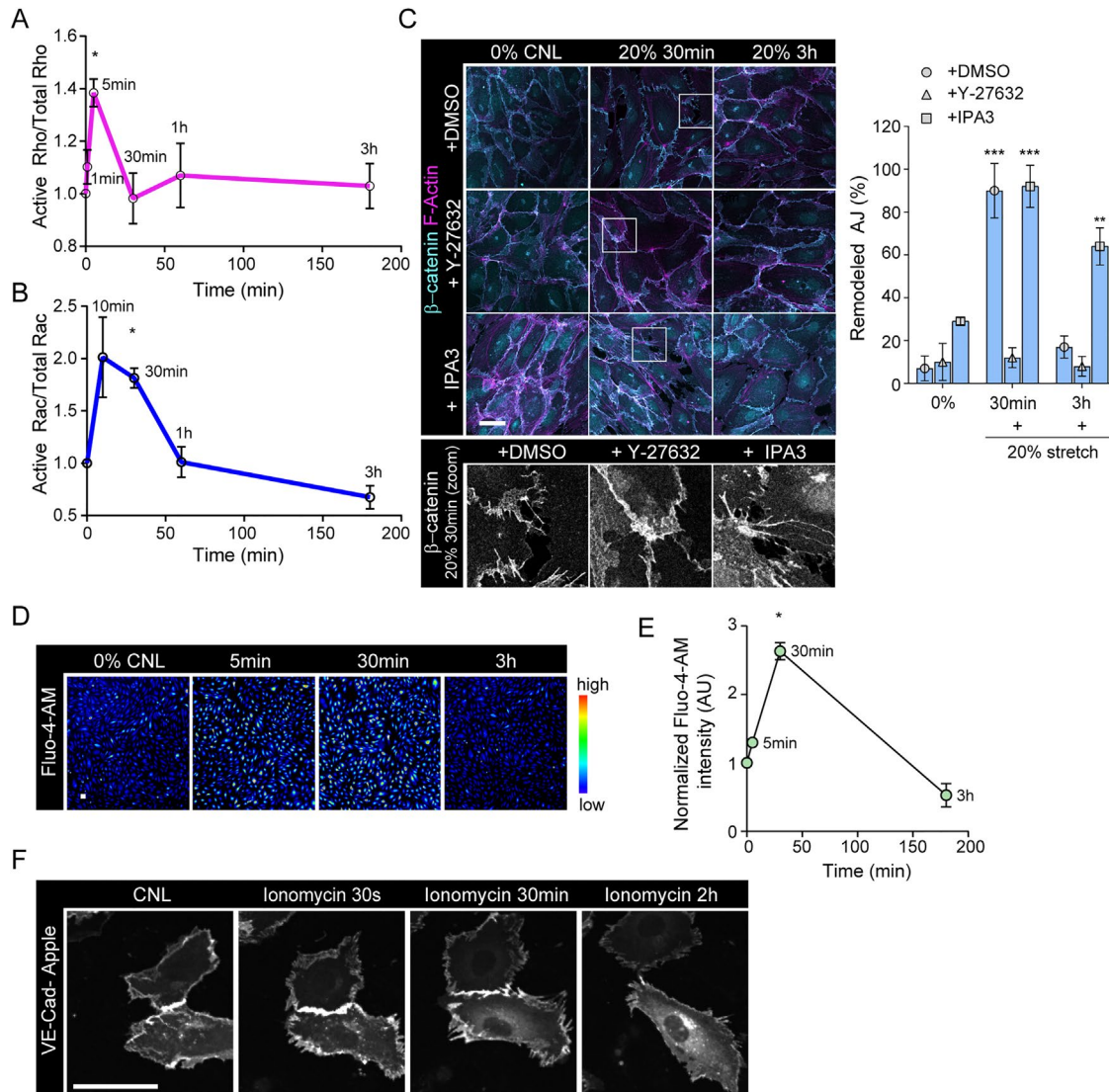


FIGURE 4: Stretch triggers transient calcium signaling and activation of Rho and GTPases to remodel junctions. (A) Quantification of RhoA activity over time shows peak of Rho activation at 5 min of stretch (mean \pm SD; $n = 3$ independent experiments; $*p = 0.0461$, ANOVA with Dunnett's). (B) Quantification of Rac1 activity over time shows peak of Rac activation at 30 min of stretch (mean \pm SD; $n = 4$ independent experiments; $*p = 0.0163$, ANOVA with Dunnett's). (C) Representative immunofluorescence images and quantification of AJ remodeling from β -catenin and F-actin (phalloidin)-stained HUVEC monolayers exposed to stretch in the presence of either Y-27632 or IPA3. Note prevention of adhesion zippering in Y-27632-treated cells and attenuated junction restoration in IPA3-treated cells. Scale bars 30 μ m (mean \pm SD; $n = 3$ independent experiments; $***p < 0.0001$, $**p = 0.0015$, ANOVA with Dunnett's). (D, E) Representative images, D, and quantification, E, of calcium imaging with Fluo-4-AM shows a transient increase in intracellular calcium at 30 min of stretch (mean \pm SD; $n = 3$ independent experiments; $*p = 0.0106$, ANOVA with Dunnett's; scale bars 30 μ m). (F) Representative immunofluorescence images of confluent, transiently VE-cadherin-Apple transfected HUVEC monolayers showing remodeling of VE-cadherin junctions in response to ionophore application. Scale bars 30 μ m.

exposed cells to cyclic stretch. Interestingly, Piezo 1 depletion attenuated elevation of pMLC2 as well as junction remodeling in response to stretch (Figure 5, C and D).

We next asked how the calcium influx could be halted despite continuous mechanical stimulus, as observed after 30–60 min of stretch (Figure 4, D and E). To this end, we analyzed Piezo 1 protein levels over time and observed that they decreased at 30 min of stretch (Figure 5, E and F). Interestingly, however, Piezo1 levels were restored to baseline at 1 h (Figure 5, E and F). Levels of Piezo mRNA were not altered significantly (Supplemental Figure 4B). We thus hypothesized that Piezo1 protein could be de-

graded in response to stretch. To this end, we blocked the proteasome and lysosome degradation pathways using MG132 and bafilomycin A1, respectively. Whereas bafilomycin A1 had no effect on Piezo1 protein levels, MG132 treatment prevented Piezo1 degradation (Supplemental Figure 4C, D), indicating that stretch triggers Piezo1 degradation via the proteasome. Collectively, these data indicated that calcium influx through Piezo1 was responsible for the stretch-induced junction remodeling, but long term this effect was attenuated through proteasome degradation of Piezo1 and subsequent return of intracellular calcium to baseline.

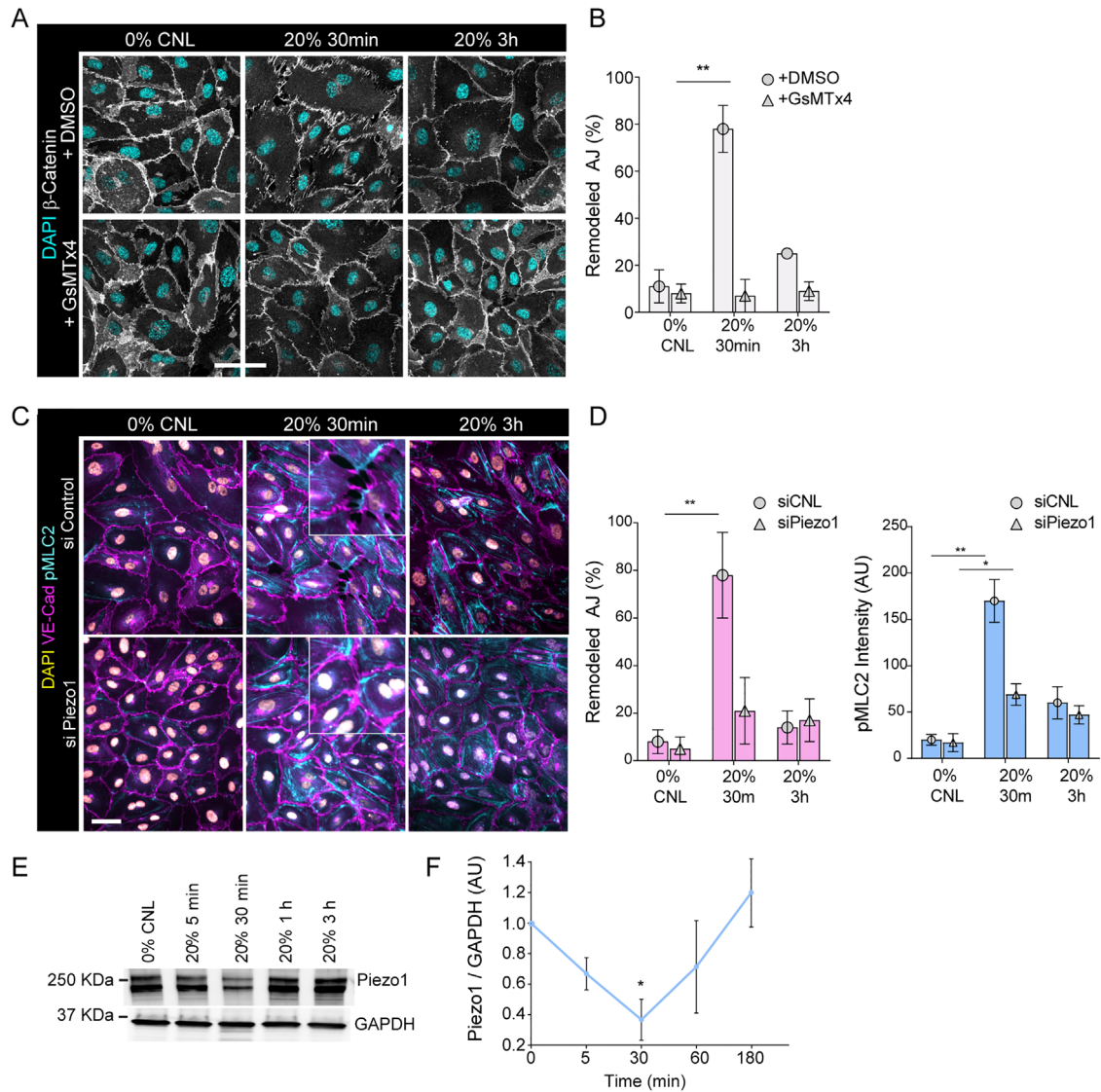


FIGURE 5: Stretch reduces Piezo1 levels to attenuate calcium signaling. (A, B) Representative immunofluorescence images, A, and quantification, B, of AJ remodeling from β -catenin stained junctions show prevention of junctional remodeling in the presence of GsMTx4 at 30 min of stretch (mean \pm SD; $n = 3$ independent experiments; $**p = 0.007$, ANOVA with Dunnett's; scale bars 30 μ m). (C, D) Representative immunofluorescence images, C, and quantification, D, of pMLC2 and AJ remodeling from VE-cadherin stained HUVECs with control or Piezo1 siRNA cells show attenuation of pMLC2 elevation and junctional remodeling in Piezo1-depleted at 30 min of stretch (mean \pm SD; $n = 3$ independent experiments; $**p = 0.0017$ for remodeled AJ and $*p = 0.0219$, $**p = 0.0014$ for pMLC2 intensity, ANOVA with Dunnett's; scale bars 30 μ m). (E, F) Representative Western blot, E, and quantification, F, show reduction of Piezo1 protein levels at 30 min of stretch (mean \pm SD; $n = 3$ independent experiments; $*p = 0.025$, ANOVA with Dunnett's).

Filamin-mediated monolayer stiffening facilitates long-term junction mechanoadaptation to stretch

As the decrease in Piezo1 levels was only transient, returning to baseline at 1 h of stretch (Figure 5, E and F), whereas at the same time intracellular calcium levels remained low (Figure 4, D and E) and junctional architecture and pMLC2 were restored (Figure 1, B–E), we hypothesized that a second, slower adaptation mechanism was being employed to prevent further calcium influx and thus to maintain junctional integrity. Recent structural studies indicate that Piezo channels are gated by membrane tension through changes in the local curvature of the membrane, tuned by cytoskeletal mechanics (Cox *et al.*, 2016; Liang and Howard, 2018), indicating that the cell cortex could play a role in regulating the sensitivity of these channels. We therefore analyzed the effects of stretch on the elastic

modulus of the cell cortex using atomic force microscopy-based force indentation spectroscopy (Muller *et al.*, 2020; Figure 6A). These analyses revealed significant stiffening of EC cortices at starting at 30 min and sustained over 3 h of stretch (Figure 6B).

To identify the cytoskeletal structure(s) responsible for this change in cortex mechanics, we inhibited actomyosin contraction (blebbistatin), actin (cytochalasin D), microtubule polymerization (nocodazole), and intermediated filament assembly (acrylamide). Interestingly, inhibiting actin polymerization with cytochalasin D had the strongest effect in preventing cortical stiffening in response to stretch, whereas blebbistatin had a much less pronounced effect, similarly to the PAK inhibitor IPA3 (Supplemental Figure 5, A and B). Also, in contrast to F-actin, the intermediate filament and microtubule cytoskeletons were not substantially remodeled in response to

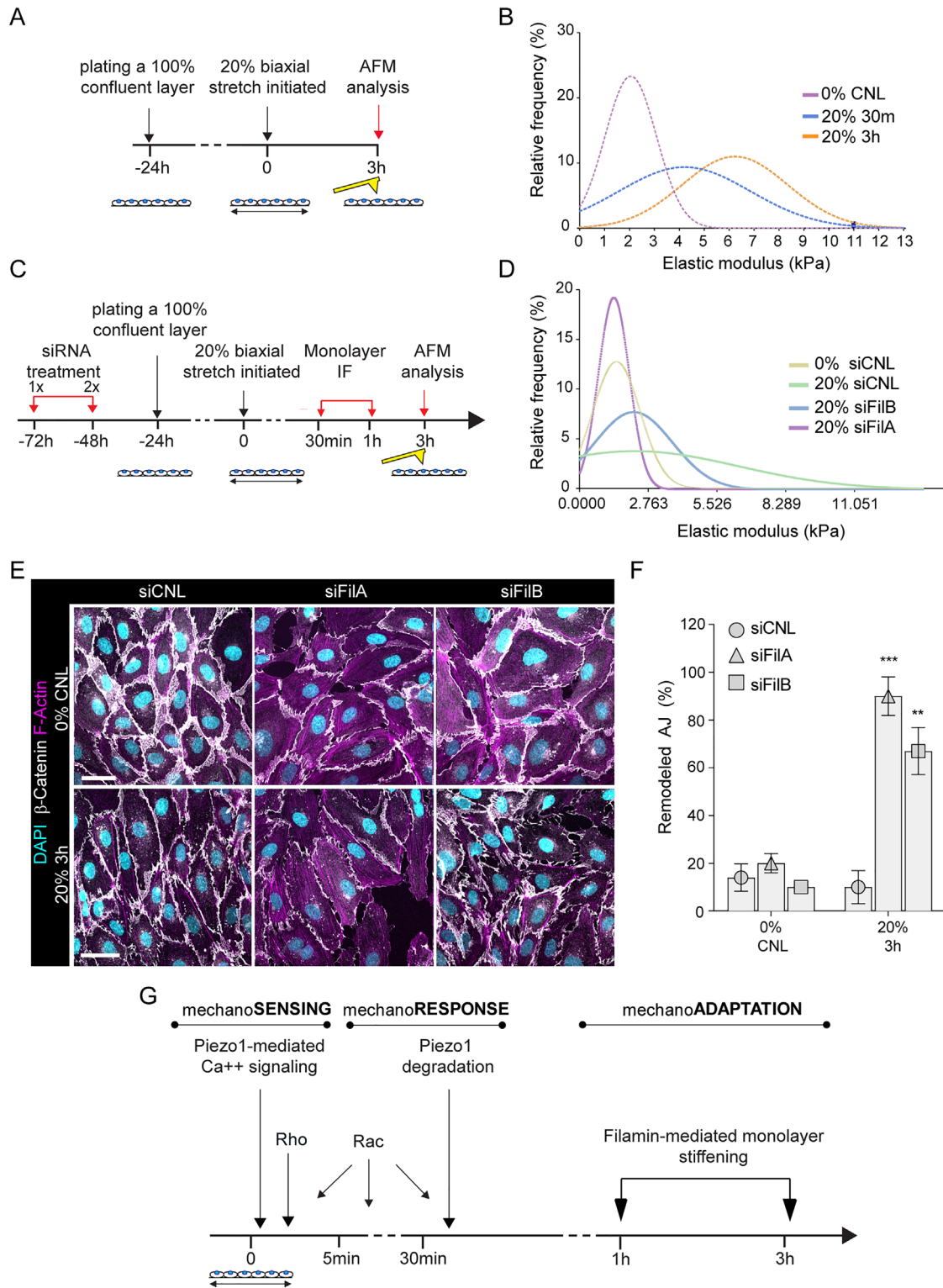


FIGURE 6: Filamin-mediated monolayer stiffening facilitates long-term junction mechanoadaptation. (A) Schematic illustration of the atomic force microscopy experiments to quantify monolayer cortical stiffness. (B) Frequency distribution of monolayer elastic moduli show stiffening in response to stretch ($n = 150\text{--}200$ force curves pooled across three independent experiments; $***p < 0.0001$, 30 min, 20% versus 0%, $**p < 0.005$, 3 h, 20% versus 0%, Kolmogorov–Smirnov test). (C) Schematic illustration of the atomic force microscopy experiments to quantify monolayer cortical stiffness in filamin-depleted cells. (D) Frequency distribution of monolayer elastic moduli shows that depletion of filamin A and to a lesser extent filamin B prevents monolayer stiffening in response to stretch ($n = 200\text{--}250$ force curves pooled across three independent experiments; $***p \leq 0.0001$, Kolmogorov–Smirnov test). (E, F) Representative immunofluorescence images, E, and quantification, F, of AJ remodeling from β -catenin show that depletion of filamin A or B prevents full restoration of adherens junction architecture at 3 h of stretch (mean \pm SD; $n = 3$ independent experiments; $***p = 0.009$, $**p = 0.0053$, ANOVA with Dunnett’s; scale bars 30 μm). (G) Model of temporal dynamics of AJ remodeling and reinforcement in response to stretch.

stretch (Supplemental Figure 5C). This indicated that F-actin reorganization was important, but most likely through mechanisms at least partially independent of the Rac-pMLC2 axis.

We had observed phosphorylation of both filamin A and B specifically after long-term (1 h) stretch (Figure 3). Filamins are mechanosensitive actin crosslinkers that have been shown to induce stretch hardening of purified F-actin networks (Tseng *et al.*, 2004; Ehrlicher *et al.*, 2011). Filamin cross-linked F-actin appears more resilient, stiffer, and less dynamic than F-actin cross-linked by α -actinin or fascin (Tseng *et al.*, 2004). To test the role of filamins in stretch-induced cortical stiffening, we depleted both proteins using siRNA (Figure 6C; Supplemental Figure 5D). Intriguingly, filamin A depletion fully prevented the stretch-induced stiffening of the cortex. Filamin B had a similar but less pronounced effect (Figure 6D). To assess if cortical stiffening was important for mechanoadaptation, we analyzed junction remodeling in filamin-depleted cells. Depletion of both filamin A and B had an effect on junctional morphology and monolayer elastic modulus (Figure 6E; Supplemental Figure 5E) already in steady state monolayers. Further, as predicted by the lack of cortical stiffening, the adaptation of the filamin-depleted cells to stretch was altered as junctions persisted in a remodeled state even after 3 h of stretch, when control cells had fully restored their architecture (Figure 6, E and F). Collectively these data indicated that filamins are phosphorylated in response to long-term stretch and contribute to cortical stiffening, facilitating adaptation of EC monolayers to high-stress environments.

DISCUSSION

Our findings show that EC monolayers respond to extrinsic biaxial stretch in a biphasic manner, first by increasing tension at adherens junctions and subsequently by cortical stiffening. The initial junction remodeling is driven by mechanosensitive calcium influx by Piezo1 and downstream GTPase signaling. Proteasomal degradation of Piezo1 facilitates restoration of junctional integrity and is followed by filamin-mediated remodeling of the actin cytoskeleton to mechanically strengthen the endothelium (Figure 6G). These findings highlight the spatiotemporally coordinated rearrangements of adhesions and the cytoskeleton to respond and adapt to high levels of mechanical stress.

The observations that cadherin bonds stiffen upon force application and that junctional composition is tension-sensitive pioneered the current understanding that cadherin molecules themselves as well as other adherens junction components are mechanosensitive and contribute to adhesion reinforcement under tension (Leckband and de Rooij, 2014; Charras and Yap, 2018). However, recent studies emphasize that mechanical cues can also induce cell–cell contact remodeling, for example, during cell migration, cell intercalation, and cell division (Pinheiro and Bellaiche, 2018), indicating that junction remodeling under tension is an equally critical process in regulating tissue architecture. We show that cyclic stretch triggers junctional remodeling as visualized by a transition of mature, linear junctions into zipperlike junctions under high tension in a process driven by Piezo1-mediated Ca^{2+} influx and downstream activation of the Rho pathway. Subsequently, Rac is activated to initiate restoration of junctions, consistent with previous studies showing that Rac stabilizes cadherin junctions (Daneshjou *et al.*, 2015). Interestingly, Rac1-Pak1 signaling has previously been implicated in remodeling/disassembly of E-cadherin-based adherens junctions in epithelial cells (Lozano *et al.*, 2008), indicating that the role of Rac signaling is most likely more complex and involves both rearrangements and mechanical strengthening. Notably, shear flow in ECs has been shown to trigger an opposite effect of decreased Rac activity

(Zaidel-Bar *et al.*, 2005), highlighting the specificity of mechanical responses to shear versus stretch and the potentially multifaceted roles of Rac signaling in this process.

Piezo1 is a mechanosensor that controls various aspects of cell behavior by allowing Ca^{2+} influx in response to extrinsic forces such as stretch, compression, and confinement (Eisenhoffer *et al.*, 2012; Li *et al.*, 2014; Nava *et al.*, 2020). Specifically in the endothelium, Piezo1 has been found to be central for mediating responses to force, including regulation of vascular maturation in the embryo (Li *et al.*, 2014), tuning blood pressure (Rode *et al.*, 2017), affecting vascular permeability (Friedrich *et al.*, 2019), impacting atherosclerosis (Albarran-Juarez *et al.*, 2018), and controlling responses to shear stress (Li *et al.*, 2014; Rode *et al.*, 2017). Intracellular Ca^{2+} in turn is a powerful second messenger capable of activating a number of signaling pathways, including the Rho and Rac pathway (Price *et al.*, 2003; Sakurada *et al.*, 2003). We observe that Piezo1-mediated Ca^{2+} , activated by cyclic stretch as expected, is involved in junction remodeling. We hypothesize that this initial junction remodeling represents a redistribution of tension to prevent cell shape changes and stress failure of the monolayer. Interestingly, similar Piezo1-mediated junctional rearrangements have been observed in ECs in response to hydrostatic pressure (Friedrich *et al.*, 2019), indicating that this might be a more general phenomenon.

Surprisingly, the integrity of junctions is restored and the Ca^{2+} influx terminated after 1–3 h of continuous stretch, indicating that the mechanosensory function of Piezo1 might be attenuated or desensitized. Analysis of Piezo1 protein levels show a transient reduction in its levels upon stretch without alterations in mRNA indicative of posttranslational regulation. Indeed, blocking proteasomal degradation prevents the reduction in Piezo1, indicating that it is removed by the proteasome. Consistently, earlier studies have implicated the ubiquitin–proteasome pathway in modulating surface expression of several ion channels, thereby altering the sensitivity of these pathways (Abriel and Staub, 2005). The precise trigger and molecular mechanism of potential ubiquitination, as well as the cellular compartment where this occurs, remain key open questions for future research.

Concomitant with the recovery of Piezo1 levels we observe monolayer strain stiffening, indicated by the elevated elastic modulus of the apical surface of the ECs. Cortical stiffness is mostly determined by cytoskeletal elements (Chugh *et al.*, 2017), and consistently we find that the actomyosin cytoskeleton and the actin cross-linkers filamin A and B play key roles. Interestingly, filamin A has been implicated in increasing cortical stiffness in response to increased substrate rigidity through enhancing the buildup of internal myosin-generated tension in the cytoskeleton, placing filamin downstream of myosin II and the actomyosin cytoskeleton in regulating cortical stiffness (Kasza *et al.*, 2009). This is consistent with the time scale of strain stiffening in our experiments, where stiffening is initiated at 30 min of stretch where myosin activity peaks. Interestingly, filamin A is mechanosensitive already at nanometer molecular deformations, and its activity generates a cross-linked, percolated actin cytoskeleton network that can transmit mechanical signals over long intracellular distances (Ehrlicher *et al.*, 2011). Our data indicate that the filamin A-mediated cortical stiffening persists beyond the peak and eventual decline in myosin phosphorylation, indicating that regulation of the cortical F-actin architecture through filamin actin cross-linking activity, independent of contractility, is likely to play a key role in mechanically reinforcing the cytoskeleton for efficient mechanoadaptation. As the sensitivity of stretch-induced ion channels to the mean stress in the cortex can be modified by alterations in scaffold proteins (Cox *et al.*, 2016), we speculate

that this increase in cortical stiffness elevates the threshold for Piezo1 activation, and this desensitization could prevent further calcium influx despite the normalization of Piezo1 protein levels in these mechanically adapted EC monolayers.

Collectively, our studies uncover a biphasic mechanical stress response characterized by rapid adhesion mechanical rearrangement, followed by monolayer mechanoadaptation to restore tissue integrity. These responses might be relevant to mitigating stress failure injury, for example, under conditions of elevated vascular pressure.

MATERIALS AND METHODS

[Request a protocol](#) through *Bio-protocol*.

Cell lines and culture

Human umbilical vein endothelial cells were purchased from Lonza and grown in EBM-2 Endothelial Cell Growth Basal Medium (Lonza). Cells were cultured in 5% CO₂ at 37°C and used between passages 2 and 4.

Mechanical stretching

Cells were plated on fibronectin-coated (20 µg/ml) culture plates with a silicon elastomer membrane (Bioflex; FlexCell International Corporation) and exposed to cyclic mechanical stretch using the Flexcell Tension System (FX4000T; FlexCell International Corporation) with indicated elongation and frequency parameters.

Chemical treatments

Where indicated, cells were treated with cytochalasin D (200 nM, Sigma-Aldrich), blebbistatin (2 µM, Sigma-Aldrich), IPA-3 (5 µM, Selleckchem), nocodazole (5 µM, Sigma-Aldrich), acrylamide (5 mM, Sigma-Aldrich), calcium ionophore A23187 (5 µM, Sigma-Aldrich), or GsMTx4 (5 µM, Tocris Bioscience). The vehicle dimethyl sulfoxide (DMSO; Sigma-Aldrich) was used as a control for all treatments.

Immunofluorescence and confocal microscopy

Cells were fixed in 4% paraformaldehyde (PFA), permeabilized with 0.3% Triton X-100 in phosphate-buffered saline (PBS), and blocked in 5% bovine serum albumin (BSA). Samples were subsequently incubated overnight in primary antibody in 1% BSA/0.3% Triton X-100/PBS, followed by washing in PBS and incubation in secondary antibody in 1% BSA/0.3% Triton X-100/PBS. Finally, samples were mounted in Elvanol. The following antibodies were used: VE-cadherin (Abcam AB33168; 1:400), β-catenin (Santa Cruz Biotechnology; sc-7199; 1:500) Phospho-Myosin Light Chain 2 (Thr18/Ser19; Cell Signaling; 3674; 1:200), vinculin (Millipore MAB 3574, 1:500), α18 (Yonemura *et al.*, 2010), 1:8000), HA-Tag (Cell Signaling 2367; 1:1000) streptavidin (ThermoFisher Scientific MA1-20010; 1:1000), and Alexa Fluor 488, 568, and 647 conjugated secondary antibodies (Invitrogen; 1:400). Actin was labeled with Alexa Fluor 488, 568, or 647-conjugated phalloidin (Invitrogen; 1:600).

All fluorescence images were collected by laser scanning confocal microscopy (SP8X; Leica) with Leica Application Suite software (LAS X version 2.0.0.14332), using 40×, 63×, or 100× immersion objectives.

Image analyses

Images were analyzed using Fiji (Schindelin *et al.*, 2012). Fields were randomly selected based exclusively on the presence of nuclei, as assessed by DAPI staining. For quantification of junction remodeling, junctions were thresholded according to VE-cadherin or β-catenin fluorescence intensity, and the coefficient of variation of intensity was computed for individual junctions. Junctions were

classified as remodeled if coefficient of variation placed into the top 30% within a dataset. For quantification of cell shapes, junctions were segmented and cell shapes were computed using the EpiTools plugin in ICY software (de Chaumont *et al.*, 2012; Heller *et al.*, 2016).

Transfections, plasmids and RNAi

siRNAs targeting hFilaminA (ID: s10058 and s10148), hFilaminB (ID: s5279 and s5278), hPiezo1 (ID: s18892 and s18893), and negative control siRNA (AM4635) were from Ambion (Silencer Select) and were transfected using RNAiMax (Invitrogen) according to manufacturers' instructions. Experiments were carried out 72 h after transfection. VE-cadherin mApple was from Addgene (#54959). pSICO-VE-Cadherin-EGFP-IRES-LifeAct-RFP was generated by subcloning human VE-cadherin cDNA from plasmid #54959 (Addgene) into the 5' of a GFP-IRES-LifeAct-RFP using the Gibson Assembly Cloning Kit (NEB). Both constructs were infected into HUVECs via lentivirus, where lentiviral particles were prepared by transfecting 293T cells with psPAX2 packaging (Addgene #12260) and pMD2.G envelope (Addgene #12259) plasmids using Lipofectamine 2000 (Invitrogen), after which the supernatant was collected and applied to cells in a 1:4 ratio with fresh media for 24 h.

Proximity-dependent biotin identification (BioID2) pulldown

Human VE-cadherin cDNA from plasmid #54959 (Addgene) was cloned into the 5' of a BioID2-HA-IRES-RFP cassette in pSicoR (#56005, Addgene) using the Gibson Assembly Cloning Kit (NEB) to generate a VE-cadherin–BioID2 fusion protein. The construct was infected into HUVECs via lentivirus, where lentiviral particles were prepared by transfecting 293T cells with psPAX2 packaging (Addgene #12260) and pMD2.G envelope (Addgene #12259) plasmids using Lipofectamine 2000 (Invitrogen), after which the supernatant was collected and applied to cells in a 1:4 ratio with fresh media for 24 h. VE-cadherin–BioID2– or BioID2 only–expressing HUVECs were stretched as described above, after which they were lysed in RIPA buffer (25 mM Tris-HCl 150 mM NaCl, 1% Nonidet P40, 0.5% sodium deoxycholate, 0.1% SDS) and sonicated using a BioRuptor sonicator (high performance with 30 s sonication/30 s pause for 10 cycles). Lysates were cleared with centrifugation and the supernatants, containing 40 mg total protein, were incubated with 100 µl of M280 Streptavidin Dynabeads (Thermo Fisher) in an end-over mixer for 8 h at 4°C to collect biotinylated proteins. Beads were subsequently washed five times with RIPA buffer and eluted with Laemmli sample buffer for analysis by Western blotting as described below. Alternatively, bound peptides were eluted from beads via incubation with 5 ng/µl Trypsin-Gold (Promega Corp., V5280) in 50 mM Tris-HCl pH7.5, 1 mM TCEP (Tris(2-carboxyethyl)phosphine), and 5 mM CAA(chloroacetamide) for 30 min at room temperature and analyzed by mass spectrometry.

Mass spectrometry

For phosphoproteomics, samples were lysed in 6 M guanidinium chloride buffer supplemented with 5 mM Tris(2-carboxyethyl)phosphine and 10 mM chloroacetamide in 100 mM Tris-HCl. Following lysis samples were heated at 95°C for 10 min, sonicated at high performance for 10 cycles (30 s on/off) using Bioruptor Plus Ultrasonicator (Diagenode), and spun down for 20 min at room temperature at 20,000 × *g*. Supernatants were then Trypsin Gold digested (Promega Corp., V5280) overnight at 37°C. Following digestion samples were acidified to block trypsin activity and peptides were cleaned with custom-packed C18-SD Stage Tips. Eluted peptides were vacuum-dried at 30°C and either subjected to LC/MS or further processed to enrich for phosphopeptides. Phosphopeptides

were enriched using the 3 mg/200 μ L Titansphere Phos-TiO kit (GL Sciences) according to manufacturer's instructions. Briefly, spin tips were assembled with centrifugal adaptors and connected to waste fluid tubes; 3000 \times g spins for 2 min at room temperature were used for all steps. Spin tips were first conditioned with 0.4% trifluoroacetic acid/80% acetonitrile solution and then equilibrated with 25% lactic acid in equilibration buffer. Peptides were then adsorbed to the spin tips, rinsed twice, and eluted with 5% ammonium hydroxide.

For BioID2 proteomics, samples were eluted from beads as described above, after which Trypsin digestion was continued overnight at 37°C.

After elution, both phosphopeptides and BioID2-eluted peptides were vacuum dehydrated for 2 h at 30°C and cleaned with custom-packed C18-SD Stage Tips. Peptides were separated on a 25-cm, 75 μ m-internal diameter PicoFrit analytical column (New Objective) packed with 1.9 μ m ReproSil-Pur 120 C18-AQ media (Dr. Maisch) using an EASY-nLC 1200 (Thermo Fisher Scientific). The column was maintained at 50°C. Buffers A and B were 0.1% formic acid in water and 0.1% formic acid in 80% acetonitrile. Peptides were separated on a segmented gradient from 6% to 31% buffer B for 120 min and then from 31% to 50% for 10 min, followed by washing and reequilibration. Eluted peptides from cells were analyzed with an Orbitrap QExactive HF mass spectrometer (Thermo Fisher Scientific). Peptide precursor *m/z* measurements were carried out at a resolution of 60,000 in the range of 300–1800 *m/z*. The 10 most intense precursors with charge state from 2 to 7 were selected for HCD fragmentation using 25% normalized collision energy. The *m/z* values of the peptide fragments were measured at a resolution of 30,000 using an AGC target of 2e5 and 55 ms maximum injection time. For phosphopeptides, an Orbitrap Fusion mass spectrometer (Thermo Fisher Scientific) was used for analyzing. Peptide precursor *m/z* measurements were carried out at a resolution of 60,000 in the range of 300–1500 *m/z*. The top speed mode was used to select precursors with charge state from 2 to 7 for HCD fragmentation using 27% normalized collision energy. The *m/z* values of the peptide fragments were measured at a resolution of 60,000 using an AGC target of 2e5 and 120 ms maximum injection time. The raw data were analyzed with MaxQuant version 1.6.1.0 using the integrated Andromeda search engine. Peptide fragmentation spectra were searched against the canonical and isoform sequences of the human reference proteome (proteome ID UP000005640, downloaded September 2018 from UniProt). Methionine oxidation and protein N-terminal acetylation were set as variable modifications; cysteine carbamidomethylation was set as fixed modification. The digestion parameters were set to "specific" and "Trypsin/P." The minimum number of peptides and razor peptides for protein identification was 1 and the minimum number of unique peptides was 0. Protein identification was performed at a peptide spectrum match and protein false discovery rate of 0.01. The "second peptide" option was on. Successful identifications were transferred between the different raw files using the "Match between runs" option. Label-free quantification (LFQ) was performed using an LFQ minimum ratio count of 2. LFQ intensities were filtered for a number of valid values that was equal to the minimum number of replicates in an experimental group minus one. Missing values were imputed from a normal distribution with a width of 0.3 and downshift of 1.8. Differential abundance analysis was performed with the Perseus statistical framework (<http://www.perseus-framework.org/>), version 1.5.2.4. After removal of the contaminants and reverse identifications, the intensities were transformed to log2. One-way ANOVA was performed to identify the significantly up- and down-regulated proteins. Benjamini–Hochberg false discovery rate 0.05 was used for truncation. GO-term

analyses were performed with DAVID and protein interaction analyses with STRING.

RhoA and Rac activity assays

Rho activity was measured with a calorimetric RhoA G-LISA activation assay kit (Cytoskeleton) according to the manufacturer's instructions.

Rac pull-downs were performed using GST-PAK-PBD as bait with the Active Rac1 Detection Kit (Cell Signaling #8815) according to the manufacturer's instructions.

Western blotting

Cells were rinsed in PBS, suspended in lysis buffer (50mM Tris-HCl buffer, pH 8.0, containing 150mM NaCl, 1% Triton X-100, 0.05% sodium deoxycholate, 10mM EDTA, and protease and phosphatase inhibitors), and cleared by centrifugation. The lysates were then reduced in Laemmli sample buffer at 95°C, separated by polyacrylamide gel electrophoresis in the presence of SDS, and transferred onto PVDF membranes. Membranes were blocked with 5% milk powder in Tris-buffered saline containing 0.05% Tween (TBS-Tween) for 1 h at room temperature, after which primary antibodies were added in 5% BSA, TBS-Tween and incubated overnight at +4°C. The membranes were subsequently washed in TBS-Tween, after which secondary horseradish peroxidase conjugated antibodies (Bio-Rad) were added in 5% milk powder in TBS-Tween and incubated for 30 min at room temperature. After extensive washing in TBS-Tween, antibody binding was detected by chemiluminescence (Immobilon Western, Millipore) using the Bio-Rad ChemiDoc Imaging System. The following antibodies were used: Piezo1 (Novus Biol. NBP1-78537; 1:1000), GAPDH (Cell Signaling; 2118L; 1:5000), Rac1 (Cytoskeleton ARC03; 1:1000), Streptavidin-HRP (DAKO P0397; 1:1000).

qPCR

Total RNA from cells was isolated using the RNeasy Plus Mini Kit, after which cDNA was synthesized using the High-Capacity cDNA Reverse Transcription Kit (Applied Biosystems). qPCR was performed on the StepOne Plus Real Time PCR System or CFX384 Touch Real Time PCR Detection System (Bio-Rad) using the DyNAmo ColorFlash SYBR Green Mix (Thermo Fisher). Gene expression changes were calculated using the comparative Ct (cycle threshold) method and normalized to B2M. The primers listed in Table 1 were used.

Live imaging of junctions and calcium imaging

Cells were transfected with VE-cadherin-mApple (Addgene #54959) or gCamp3 (Addgene #22692) or incubated with Fluo-4-AM Calcium day (Invitrogen) for 10 min at 37°C, washed twice with PBS, and imaged in fresh medium 20 min poststaining. Live images were captured with an Axio Observer (Zeiss) microscope, a CSU10 spinning-disk confocal scanhead (Yokogawa), and an ORCA Flash 4.0 camera (Hamamatsu), with a 25 \times oil objective. Acquisition was controlled by Visiview software. Images were collected at 37°C, 5% CO₂.

Force indentation spectroscopy

Atomic force indentation spectroscopy experiments were performed with a Bioscope II head (Veeco) mounted on an Olympus IX73 microscope. Silicon nitride cantilevers (MLCT, Bruker Daltonics) with a nominal spring constant of 0.03 N/m were used. For all indentation experiments, forces of up to 2 nN were applied, and the velocities of cantilever approach and retraction were kept constant at 2 μ m/sec ensuring detection of elastic properties only. Data analysis was carried out as described previously (Miroshnikova et al., 2018).

Gene Name	Forward Primer	Reverse Primer
B2M	GAGTATGCCTGCCGTGTGAA	GCTTACATGTCTCGATCCCCT
Piezo1	GeneCopoeia All-in-One™ qPCR primer for human PIEZO1	N/A
Piezo2	GeneCopoeia All-in-One™ qPCR primer for human PIEZO2	N/A
FilaminA	Filamin A (FLNA) human qPCR primer pair (NM_001456)	N/A
FilaminB	Filamin B (FLNB) human qPCR primer pair (NM_001457)	N/A

TABLE 1: List of primers.

Statistics and reproducibility

Statistical analyses were performed using GraphPad Prism software (GraphPad, version 5.0). Statistical significance was determined by the Mann–Whitney U-test, Student's *t* test, Kruskal–Wallis ANOVA with Dunn's post hoc test, linear regression, Wilcoxon rank, or Spearman's rank correlation coefficient test as indicated in the corresponding figure legends. In all cases where a test for normally distributed data was used, normal distribution was confirmed with the D'Agostino–Pearson omnibus test.

All experiments presented in the manuscript were repeated at least in three independent experiments/ biological replicates.

Code availability

All custom code is available from the corresponding author on request.

Data availability

All data supporting the findings of this study are available from the corresponding author on reasonable request.

ACKNOWLEDGMENTS

We thank Anu M. Luoto for technical assistance, the FACS and Imaging Core Facility of MPI for Biology of Ageing, the Biomedicum Imaging Unit for support with imaging, and Akira Nafaguchi for the α -18 antibody. This work was supported by the Whitaker postdoctoral fellowship, EMBO Long-Term fellowship ALTF 728-2017, and Human Frontier Science Program fellowship LT000861/2018 (to Y.A.M.), the Sigrid Juselius Foundation, Max Planck Society, and Helsinki Institute of Life Science (to S.A.W.), and the Fondation pour la Recherche Medicale (DEQ20170336702) and Agence Nationale de la Recherche (ANR-17-CE13-022; to C.A.R.).

REFERENCES

Abriel H, Staub O (2005). Ubiquitylation of ion channels. *Physiology* (Bethesda) 20, 398–407.

Acharya BR, Nestor-Bergmann A, Liang X, Gupta S, Duszyc K, Gauquelin E, Gomez GA, Budnar S, Marcq P, Jensen OE, *et al.* (2018). A mechanosensitive RhoA pathway that protects epithelia against acute tensile stress. *Dev Cell* 47, 439–452 e436.

Albarran-Juarez J, Iring A, Wang S, Joseph S, Grimm M, Strlic B, Wetschurck N, Althoff TF, Offermanns S (2018). Piezo1 and Gq/G11 promote endothelial inflammation depending on flow pattern and integrin activation. *J Exp Med* 215, 2655–2672.

Bae C, Sachs F, Gottlieb PA (2011). The mechanosensitive ion channel Piezo1 is inhibited by the peptide GsMTx4. *Biochemistry* 50, 6295–6300.

Baeyens N, Schwartz MA (2016). Biomechanics of vascular mechanosensation and remodeling. *Mol Biol Cell* 27, 7–11.

Beech DJ, Kalli AC (2019). Force Sensing by piezo channels in cardiovascular health and disease. *Arterioscler Thromb Vasc Biol* 39, 2228–2239.

Brzeska H, Szczepanowska J, Matsumura F, Korn ED (2004). Rac-induced increase of phosphorylation of myosin regulatory light chain in HeLa cells. *Cell Motil Cytoskeleton* 58, 186–199.

Charras G, Yap AS (2018). Tensile forces and mechanotransduction at cell–cell junctions. *Curr Biol* 28, R445–R457.

Chugh P, Clark AG, Smith MB, Cassani DAD, Dierkes K, Ragab A, Roux PP, Charras G, Salbreux G, Paluch EK (2017). Actin cortex architecture regulates cell surface tension. *Nat Cell Biol* 19, 689–697.

Cox CD, Bae C, Ziegler L, Hartley S, Nikolova-Krstevski V, Rohde PR, Ng CA, Sachs F, Gottlieb PA, Martinac B (2016). Removal of the mechanoprotective influence of the cytoskeleton reveals PIEZO1 is gated by bilayer tension. *Nat Commun* 7, 10366.

Daneshjoui N, Sieracki N, van Nieuw Amerongen GP, Conway DE, Schwartz MA, Komarova YA, Malik AB (2015). Rac1 functions as a reversible tension modulator to stabilize VE-cadherin trans-interaction. *J Cell Biol* 208, 23–32.

de Chaumont F, Dallongeville S, Chenouard N, Herve N, Pop S, Provoost T, Meas-Yedid V, Pankajakshan P, Lecomte T, Le Montagner Y, *et al.* (2012). Icy: an open bioimage informatics platform for extended reproducible research. *Nat Methods* 9, 690–696.

Dorland YL, Huveneres S (2017). Cell–cell junctional mechanotransduction in endothelial remodeling. *Cell Mol Life Sci* 74, 279–292.

Dufour S, Mege RM, Thiery JP (2013). Alpha-catenin, vinculin, and F-actin in strengthening E-cadherin cell–cell adhesions and mechanosensing. *Cell Adh Migr* 7, 345–350.

Ehrlicher AJ, Nakamura F, Hartwig JH, Weitz DA, Stossel TP (2011). Mechanical strain in actin networks regulates FilGAP and integrin binding to filamin A. *Nature* 478, 260–263.

Eisenhoffer GT, Loftus PD, Yoshigi M, Otsuna H, Chien CB, Morcos PA, Rosenblatt J (2012). Crowding induces live cell extrusion to maintain homeostatic cell numbers in epithelia. *Nature* 484, 546–549.

Friedrich EE, Hong Z, Xiong S, Zhong M, Di A, Rehman J, Komarova YA, Malik AB (2019). Endothelial cell Piezo1 mediates pressure-induced lung vascular hyperpermeability via disruption of adherens junctions. *Proc Natl Acad Sci USA* 116, 12980–12985.

Haga JH, Li YS, Chien S (2007). Molecular basis of the effects of mechanical stretch on vascular smooth muscle cells. *J Biomech* 40, 947–960.

Hahn C, Schwartz MA (2009). Mechanotransduction in vascular physiology and atherogenesis. *Nat Rev Mol Cell Biol* 10, 53–62.

Heller D, Hoppe A, Restrepo S, Gatti L, Tournier AL, Tapon N, Basler K, Mao Y (2016). EpiTools: an open-source image analysis toolkit for quantifying epithelial growth dynamics. *Dev Cell* 36, 103–116.

Hoffman BD, Grashoff C, Schwartz MA (2011). Dynamic molecular processes mediate cellular mechanotransduction. *Nature* 475, 316–323.

Huveneres S, Oldenburg J, Spanjaard E, van der Krogt G, Grigoriev I, Akhmanova A, Rehmann H, de Rooij J (2012). Vinculin associates with endothelial VE-cadherin junctions to control force-dependent remodeling. *J Cell Biol* 196, 641–652.

Iskratsch T, Wolfenson H, Sheetz MP (2014). Appreciating force and shape—the rise of mechanotransduction in cell biology. *Nat Rev Mol Cell Biol* 15, 825–833.

Jufri NF, Mohamedali A, Avolio A, Baker MS (2015). Mechanical stretch: physiological and pathological implications for human vascular endothelial cells. *Vasc Cell* 7, 8.

Kasza KE, Nakamura F, Hu S, Kollmannsberger P, Bonakdar N, Fabry B, Stossel TP, Wang N, Weitz DA (2009). Filamin A is essential for active cell stiffening but not passive stiffening under external force. *Biophys J* 96, 4326–4335.

Kim J, Cooper JA (2018). Septins regulate junctional integrity of endothelial monolayers. *Mol Biol Cell* 29, 1693–1703.

Konishi S, Yano T, Tanaka H, Mizuno T, Kanoh H, Tsukita K, Namba T, Tamura A, Yonemura S, Gotoh S, *et al.* (2019). Vinculin is critical for the robustness of the epithelial cell sheet paracellular barrier for ions. *Life Sci Alliance* 2.

Krishnan R, Klumpers DD, Park CY, Rajendran K, Treppe X, van Bezu J, van Hinsbergh VW, Carman, CV, Brain JD, Fredberg JJ, *et al.* (2011). Substrate stiffening promotes endothelial monolayer disruption through enhanced physical forces. *Am J Physiol Cell Physiol* 300, C146–C154.

- le Duc Q, Shi Q, Blonk I, Sonnenberg A, Wang N, Leckband D, de Rooij J (2010). Vinculin potentiates E-cadherin mechanosensing and is recruited to actin-anchored sites within adherens junctions in a myosin II-dependent manner. *J Cell Biol* 189, 1107–1115.
- Leckband DE, de Rooij J (2014). Cadherin adhesion and mechanotransduction. *Annu Rev Cell Dev Biol* 30, 291–315.
- Li J, Hou B, Tumova S, Muraki K, Bruns A, Ludlow MJ, Sedo A, Hyman AJ, McKeown L, Young RS, et al. (2014). Piezo1 integration of vascular architecture with physiological force. *Nature* 515, 279–282.
- Liang X, Howard J (2018). Structural biology: piezo senses tension through curvature. *Curr Biol* 28, R357–R359.
- Lipowsky HH, Kovalcheck S, Zweifach BW (1978). The distribution of blood rheological parameters in the microvasculature of cat mesentery. *Circ Res* 43, 738–749.
- Liu C, Hermann TE (1978). Characterization of ionomycin as a calcium ionophore. *J Biol Chem* 253, 5892–5894.
- Lock JT, Parker I, Smith IF (2015). A comparison of fluorescent Ca(2+)(+) indicators for imaging local Ca(2+)(+) signals in cultured cells. *Cell Calcium* 58, 638–648.
- Logsdon EA, Finley SD, Popel AS, Mac Gabhann F (2014). A systems biology view of blood vessel growth and remodeling. *J Cell Mol Med* 18, 1491–1508.
- Lozano E, Frasa MA, Smolarczyk K, Knaus UG, Braga VM (2008). PAK is required for the disruption of E-cadherin adhesion by the small GTPase Rac. *J Cell Sci* 121, 933–938.
- Miroshnikova YA, Le HQ, Schneider D, Thalheim T, Rubsam M, Bremicker N, Polleux J, Kamprad N, Tarantola M, Wang I, et al. (2018). Adhesion forces and cortical tension couple cell proliferation and differentiation to drive epidermal stratification. *Nat Cell Biol* 20, 69–80.
- Muller DJ, Dumitru AC, Lo Giudice C, Gaub HE, Hinterdorfer P, Hummer G, De Yoreo JJ, Dufrene YF, Alsteens D (2020). Atomic force microscopy-based force spectroscopy and multiparametric imaging of biomolecular and cellular systems. *Chem Rev*.
- Nava MM, Miroshnikova YA, Biggs LC, Whitefield DB, Metge F, Boucas J, Vihinen H, Jokitalo E, Li X, Garcia Arcos JM, et al. (2020). Heterochromatin-driven nuclear softening protects the genome against mechanical stress-induced damage. *Cell* 181, 800–817 e822.
- Ohgushi M, Matsumura M, Eiraku M, Murakami K, Aramaki T, Nishiyama A, Muguruma K, Nakano T, Suga H, Ueno M, et al. (2010). Molecular pathway and cell state responsible for dissociation-induced apoptosis in human pluripotent stem cells. *Cell Stem Cell* 7, 225–239.
- Pinheiro D, Bellaiche Y (2018). Mechanical force-driven adherens junction remodeling and epithelial dynamics. *Dev Cell* 47, 3–19.
- Price LS, Langeslag M, ten Klooster JP, Hordijk PL, Jalink K, Collard JG (2003). Calcium signaling regulates translocation and activation of Rac. *J Biol Chem* 278, 39413–39421.
- Rode B, Shi J, Endesh N, Drinkhill MJ, Webster PJ, Lotteau SJ, Bailey MA, Yuldasheva NY, Ludlow MJ, Cubbon RM, et al. (2017). Piezo1 channels sense whole body physical activity to reset cardiovascular homeostasis and enhance performance. *Nat Commun* 8, 350.
- Sakurada S, Takuwa N, Sugimoto N, Wang Y, Seto M, Sasaki Y, Takuwa Y (2003). Ca²⁺-dependent activation of Rho and Rho kinase in membrane depolarization-induced and receptor stimulation-induced vascular smooth muscle contraction. *Circ Res* 93, 548–556.
- Schindelin J, Arganda-Carreras I, Frise E, Kaynig V, Longair M, Pietzsch T, Preibisch S, Rueden C, Saalfeld S, Schmid B, et al. (2012). Fiji: an open-source platform for biological-image analysis. *Nat Methods* 9, 676–682.
- Tseng Y, An KM, Esue O, Wirtz D (2004). The bimodal role of filamin in controlling the architecture and mechanics of F-actin networks. *J Biol Chem* 279, 1819–1826.
- Twiss F, Le Duc Q, Van Der Horst S, Tabdili H, Van Der Krogt G, Wang N, Rehmann H, Huvneers S, Leckband DE, De Rooij J (2012). Vinculin-dependent cadherin mechanosensing regulates efficient epithelial barrier formation. *Biol Open* 1, 1128–1140.
- van Buul JD, Geerts D, Huvneers S (2014). Rho GAPs and GEFs: controlling switches in endothelial cell adhesion. *Cell Adh Migr* 8, 108–124.
- Vespa A, D'Souza SJ, Dagnino L (2005). A novel role for integrin-linked kinase in epithelial sheet morphogenesis. *Mol Biol Cell* 16, 4084–4095.
- Yonemura S, Wada Y, Watanabe T, Nagafuchi A, Shibata M (2010). Alpha-catenin as a tension transducer that induces adherens junction development. *Nat Cell Biol* 12, 533–542.
- Zaidel-Bar R, Kam Z, Geiger B (2005). Polarized downregulation of the paxillin-p130CAS-Rac1 pathway induced by shear flow. *J Cell Sci* 118, 3997–4007.
- Zhang H, Landmann F, Zahreddine H, Rodriguez D, Koch M, Labouesse M (2011). A tension-induced mechanotransduction pathway promotes epithelial morphogenesis. *Nature* 471, 99–103.